nature climate change

Supplementary information https://doi.org/10.1038/s41558-024-01957-9

Historical impacts of grazing on carbon stocks and climate mitigation opportunities

In the format provided by the authors and unedited

Table of Contents

Supplementary Discussion

1. Uncertainties in various input data sets

In this study, we used the ratio of grazed biomass to aboveground net primary production (ANPP) available for grazing as an indicator of grazing intensity (GI), overcoming limitations associated with the estimates of ANPP (see Methods). The improved methodology allowed us to provide more accurate GI estimates than previous literature. In particular, while we derived global observational ANPP based on recent research[1], other grazing studies used climate as predictors or a constant global value of 0.6 to derive the aboveground fraction from NPP[2,3]. To assess the reliability of our GI estimates, we performed an additional analysis. In this analysis, we used the Global Assessment of Soil Degradation (GLASOD) database as a reference[4], which provides global land degradation severity due to grazing based on expert assessment and knowledge. Specifically, the GLASOD classifies overgrazing severity into light, moderate, heavy and extreme, using a combination of the degree and the relative extent of the process. Using the same approach and spatial coverage as the GLASOD, we derived our own map of overgrazing severity based on our global GI and grazing extent maps, and found that the spatial patterns are comparable to those of GLASOD (Figure S26).

Notably, uncertainties remain in our results. Specifically, there are certain regions where GI >100% (southern Asia and northern Africa) or our severity levels deviate from the GLASOD (e.g., southern Africa and western Asia). However, it should also be kept in mind that our degree of overgrazing is defined according to productivity loss, while the GLASOD surveys focused on soil degradation. More importantly, the GLASOD is likely to be broadly accurate, but is less certain at any particular location[5]. Regardless, further efforts are required to minimize uncertainties in various input data sets, including more precise grazing fraction and ANPP maps, along with explicit feed intake data at finer scales.

There are also considerable uncertainties between the various data sets used in our study (e.g., soil properties). For example, notable discrepancies in soil carbon stocks between SoilGrids and the Harmonized World Soil Database are present, particularly in northern regions[6], which probably leads to larger coefficients of variation in carbon sequestration potential across the boreal ecozone (Table S3).

2. Robustness, reliability of GI_{opt} and GI_{thres} estimates

We performed the following analysis to assess the robustness and reliability of our results. First, we derived GI_{opt} and GI_{thres} without considering environmental factors within the moving window. By comparing with the default estimates (Figure 5), we can assess the potential influence of diverse environments within the moving windows. The results showed that the effect of diverse environments within the window is small for the vast majority of the world (Figure S27).

We also estimated GI_{opt} at a plot level from 12 field experiments (Figure S28). These experiments measured carbon stocks for aboveground plant, root and soil under at least 3 GI gradients that cover light, moderate and heavy intensities. Where studies only measured biomass, we converted to carbon stocks using a default conversion factor of 0.47[7]. Comparing these plot-level GI_{opt} estimates with those extracted from our optimal map, we found a good agreement between the two (Figure S28). However, due to the lack of data from multiple intensity gradients in these experiments, we were unable to derive definitive plot-level GI_{thres}. Nevertheless, a recent study using a process-based model investigated stocking rate thresholds (sheep unit/ha/yr) that induce extreme grassland NPP degradation over the Tibetan Plateau of China[8]. We compared these to those converted from our GI_{thres} estimates and found them to be comparable in terms of both patterns and values (Figure S29).

References

1. Xiao, L.J., et al. Global depth distribution of belowground net primary productivity and its drivers. Global Ecology and Biogeography 32, 1435-1451 (2023).
2. Fetzel, T., et al. Quantification of uncertainties in global grazing systems assessment. Global Biogeochemical Cycles 31, 1089-1102 (2017).
3. Piipponen, J., et al. Global trends in grassland carrying capacity and relative stocking density of livestock. Global Change Biology 28, 3902-3919 (2022).
4. Oldeman L R, Hakkeling R T A, Sombroek W G, et al. Global assessment of human-induced soil degradation (GLASOD). World map of the status of human-induced soil degradation, 1991.
5. Chang J, Ciais P, Gasser T, et al. Climate warming from managed grasslands cancels the cooling effect of carbon sinks in sparsely grazed and natural grasslands, Nature Communications, 12, 118. 2021.
6. Tifafi, M., Guenet, B. & Hatté, C. Large differences in global and regional total soil carbon stock estimates based on SoilGrids, HWSD, and NCSCD: Intercomparison and evaluation based on field data from USA, England, Wales, and France. Global Biogeochemical Cycles 32, 42-56 (2018).

7. Cook-Patton S C, Leavitt S M, Gibbs D, et al. Mapping carbon accumulation potential from global natural forest regrowth. Nature, 2020, 585(7826): 545-550.
8. Zhu Q, Chen H, Peng C, et al. An early warning signal for grassland degradation on the Qinghai-Tibetan Plateau. Nature Communications, 2023, 14(1): 6406.

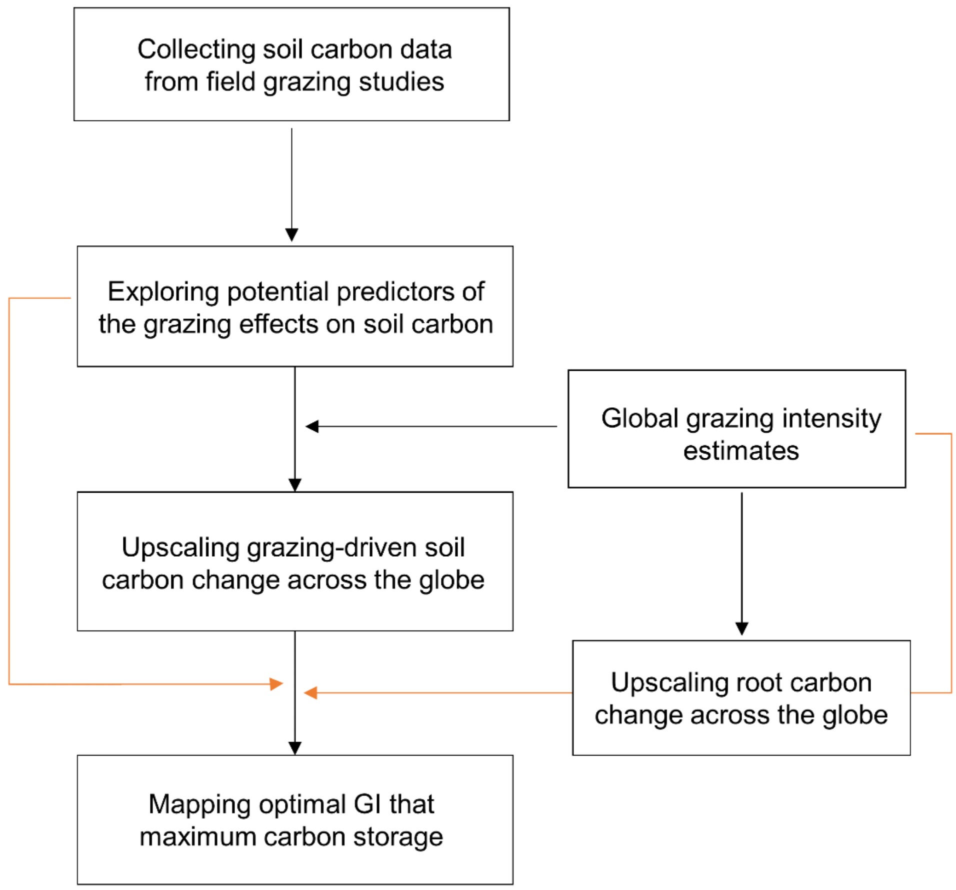

Figure S1. Flowchart showing the key steps of this study.

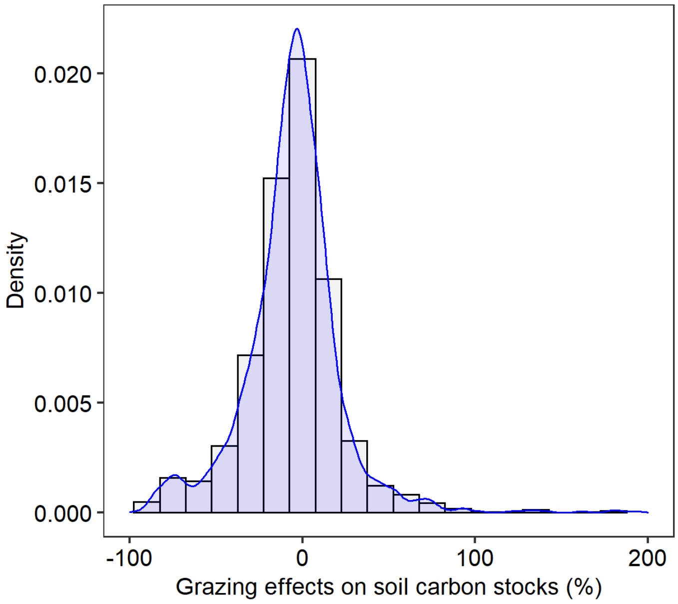

Figure S2. Density plot of the grazing effects on soil carbon stocks over 1,473 observations.

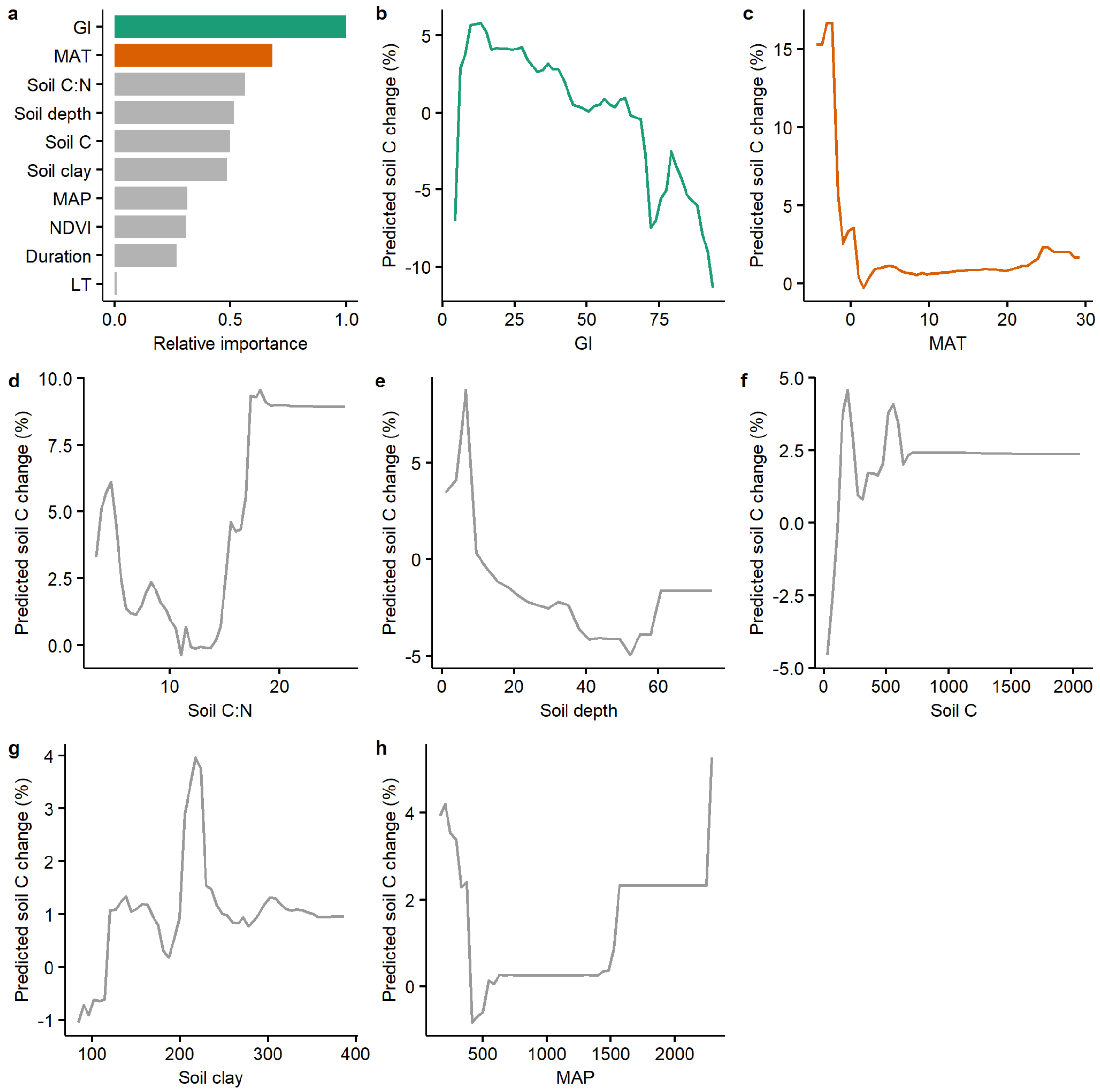

Figure S3. Variable importance of 10 potential predictors of the grazing effects on soil carbon stocks and partial dependence plots. LT, livestock types.

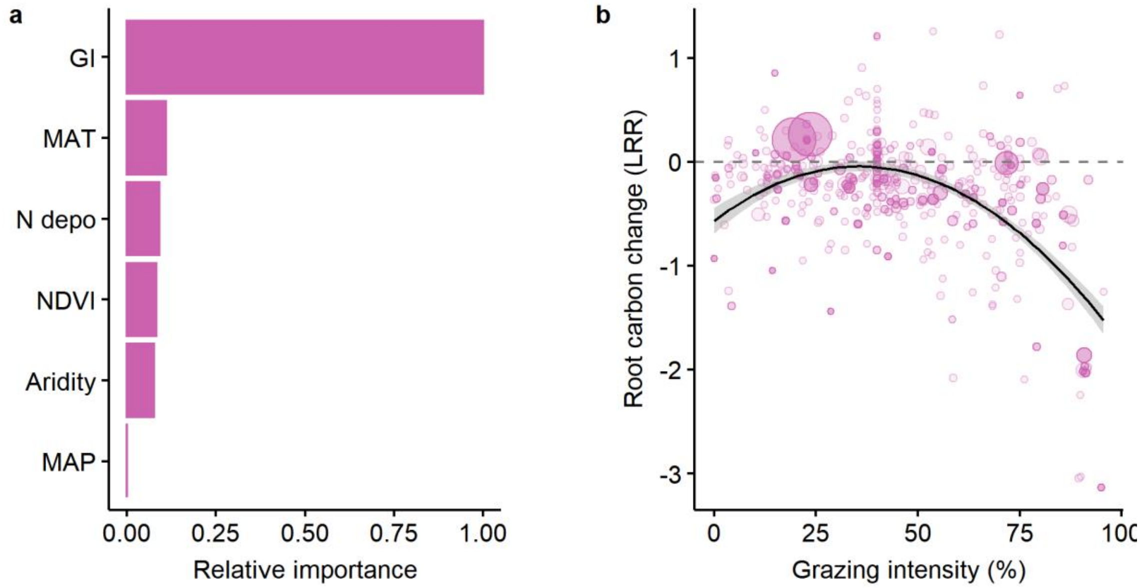

Figure S4. Grazing intensity is a key driver of the grazing-induced root carbon change. a, Variable importance of 6 factors of the grazing effects on root carbon across field observations. **b**, Regression plot of grazing intensity with root carbon change fitted by a meta-regression model ($P < 0.001$, $n = 738$; P value for two-tailed test). Data shown in **b** here are from field grazing experiments. Nonlinear fit depicts quadratic meta-regression model with shaded areas representing 95% CI.

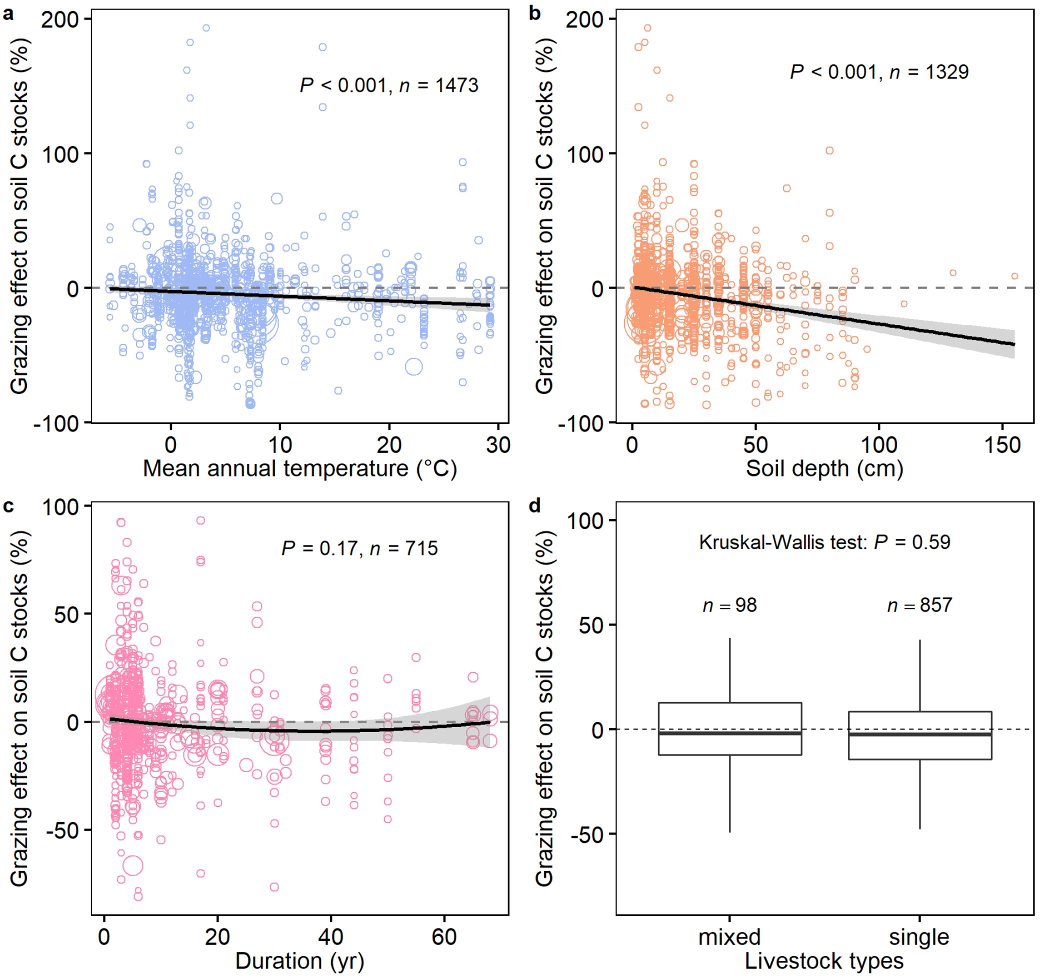

Figure S5. The influence of mean annual temperature (a, *P* = 0.0009), soil depth (b, *P* = 0.000), duration (c) and livestock types (d) on grazing-induced changes in soil carbon stocks. Data shown here are from field grazing experiments. Linear or Nonlinear fits in **a-c** represent meta-regression models with shaded areas representing 95% CI. Box plot shows the 25th and 75th percentiles (box borders), medians (central black lines) and data ranges (whiskers). *P* values for two-tailed tests.

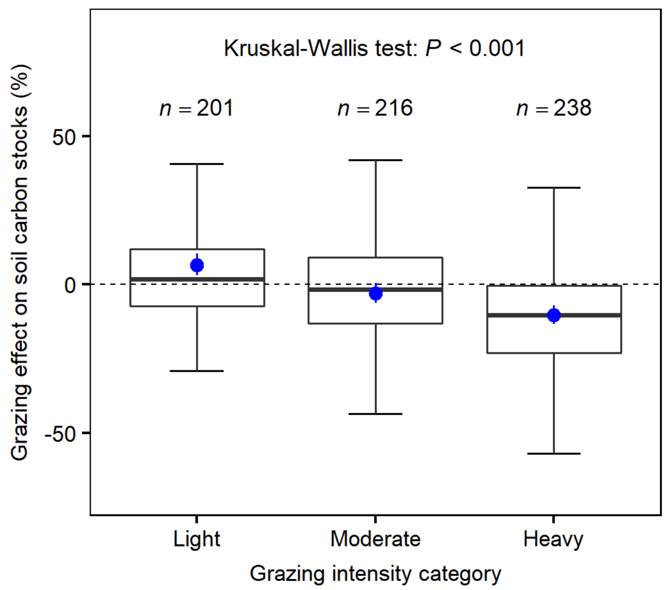

Figure S6. Comparison of the grazing effects on soil carbon stocks between light, moderate and heavy grazing intensity categories in experiments reporting the three intensity categories simultaneously (*P* = 0.000). Dots represent overall means from a meta-analysis with 95% CI. Box plot shows the 25th and 75th percentiles (box borders), medians (central black lines) and data ranges (whiskers). Data presented here are from field grazing experiments.

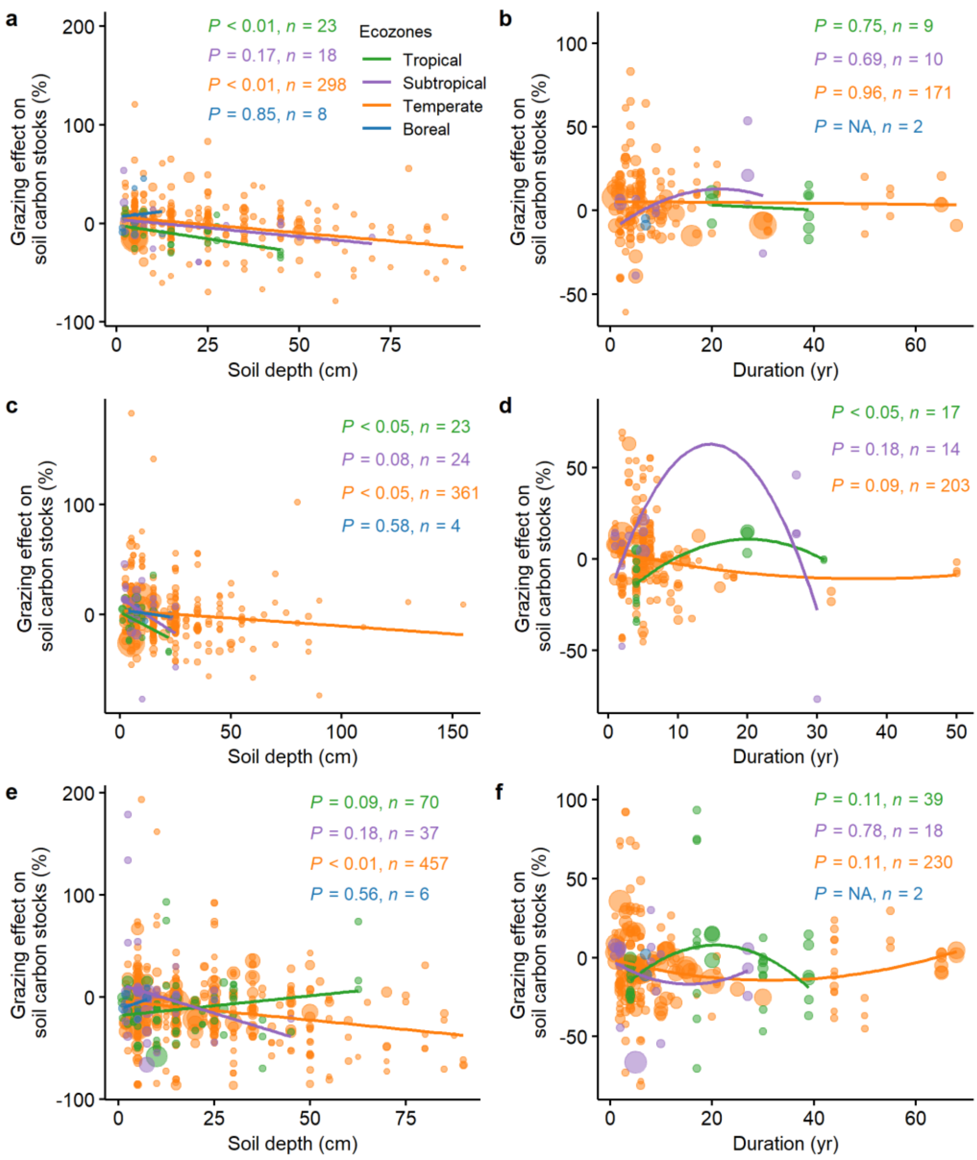

Figure S7. Regression plots of grazing effect on soil carbon stocks with soil depth and duration within light (a-b), moderate (c-d) and heavy intensity (e-f). Dot sizes are proportional to model weights. Data shown here are from field grazing experiments. Linear or Nonlinear fits depict meta-regression models with shaded areas representing 95% CI. *P* value is 0.007 and 0.000 for tropical and temperate ecozones in **a**, 0.02 and 0.001 for tropical and temperate ecozones in **c**, 0.02 for tropical ecozone in **d**, 0.000 for temperate ecozone in **e**. *P* values for two-tailed tests.

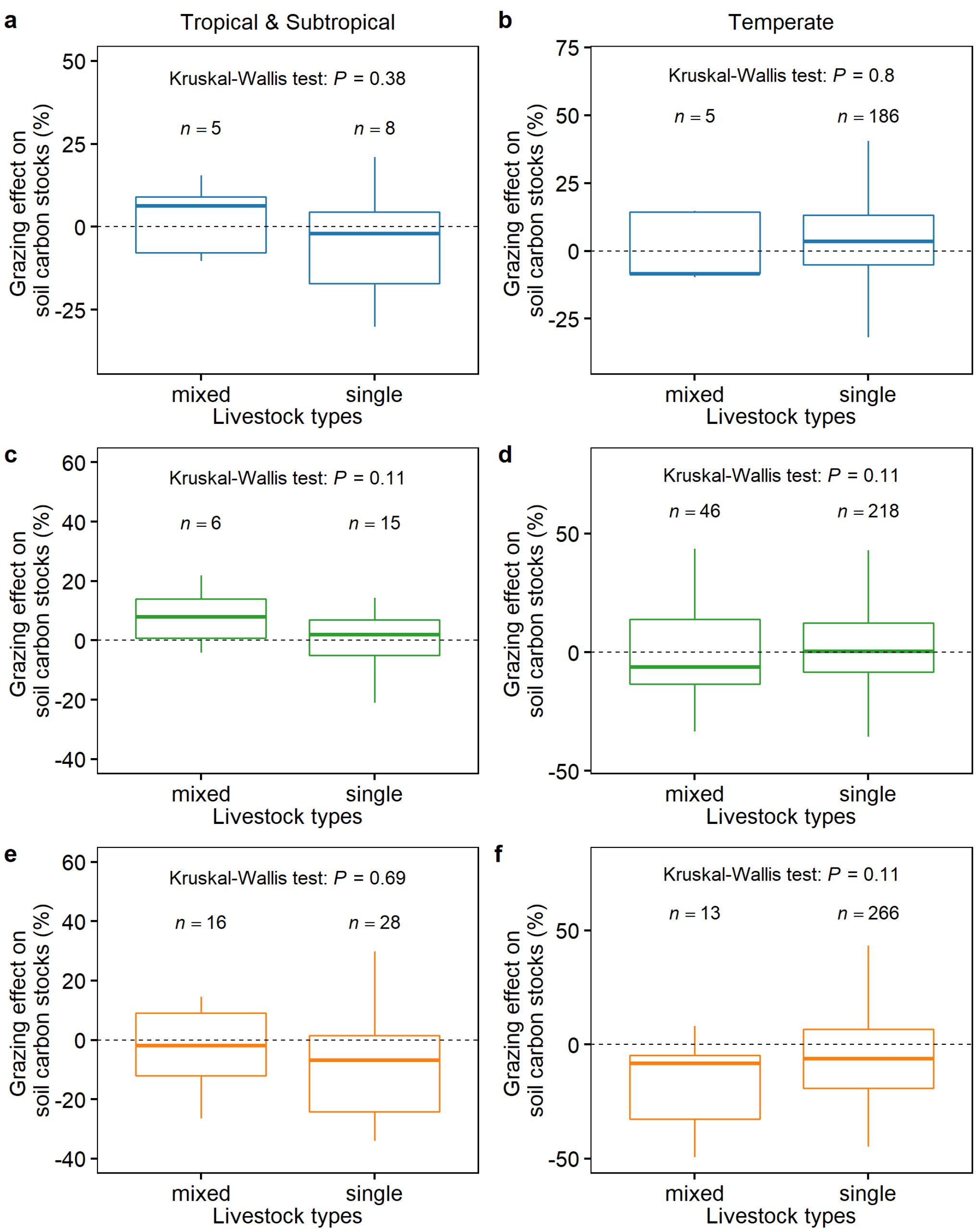

Figure S8. Comparison of the grazing effects on soil carbon stocks between different livestock types per intensity category and ecozone. a-f, Effects of livestock types on soil carbon changes for light (**a-b**), moderate (**c-d**) and heavy (**e-f**) grazing intensities. Box plots show the 25th and 75th percentiles (box borders), medians (central black lines) and data ranges (whiskers). Data shown here are from field grazing experiments.

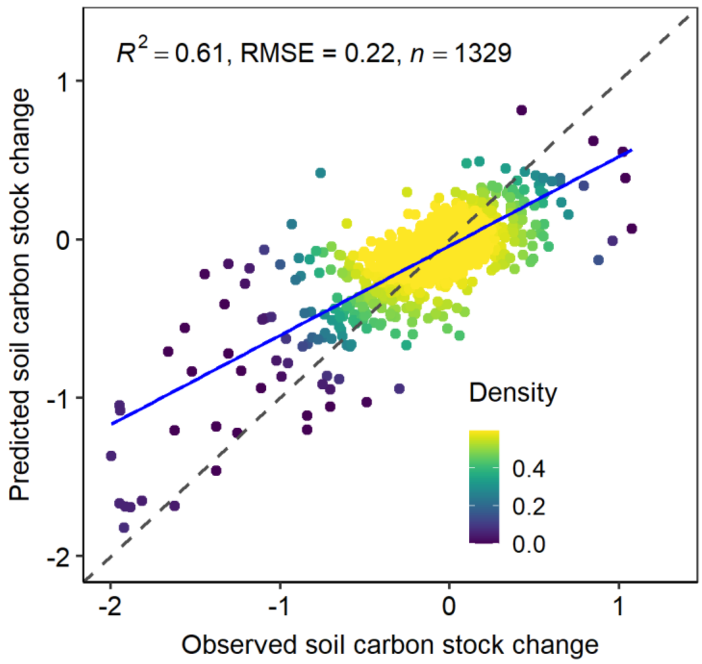

Figure S9. Heat plot showing the relationship between observed and predicted grazing-induced soil carbon stock change (LRR). Solid line indicates fitted relationship based on ordinary least squares regression; dashed line indicates a 1:1 relationship between observed and predicted points.

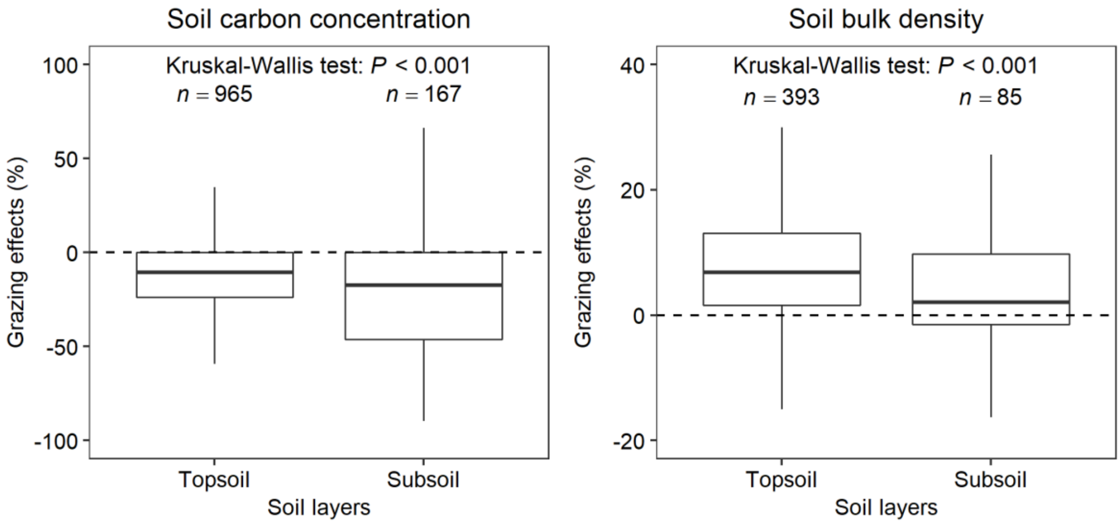

Figure S10. Comparison of the grazing effects on soil carbon content and bulk density between different layers. *P* value is 0.0008 for soil carbon content and 0.0004 for soil bulk density. Box plots show the 25th and 75th percentiles (box borders), medians (central black lines) and data ranges (whiskers). The data shown here are from field grazing experiments.

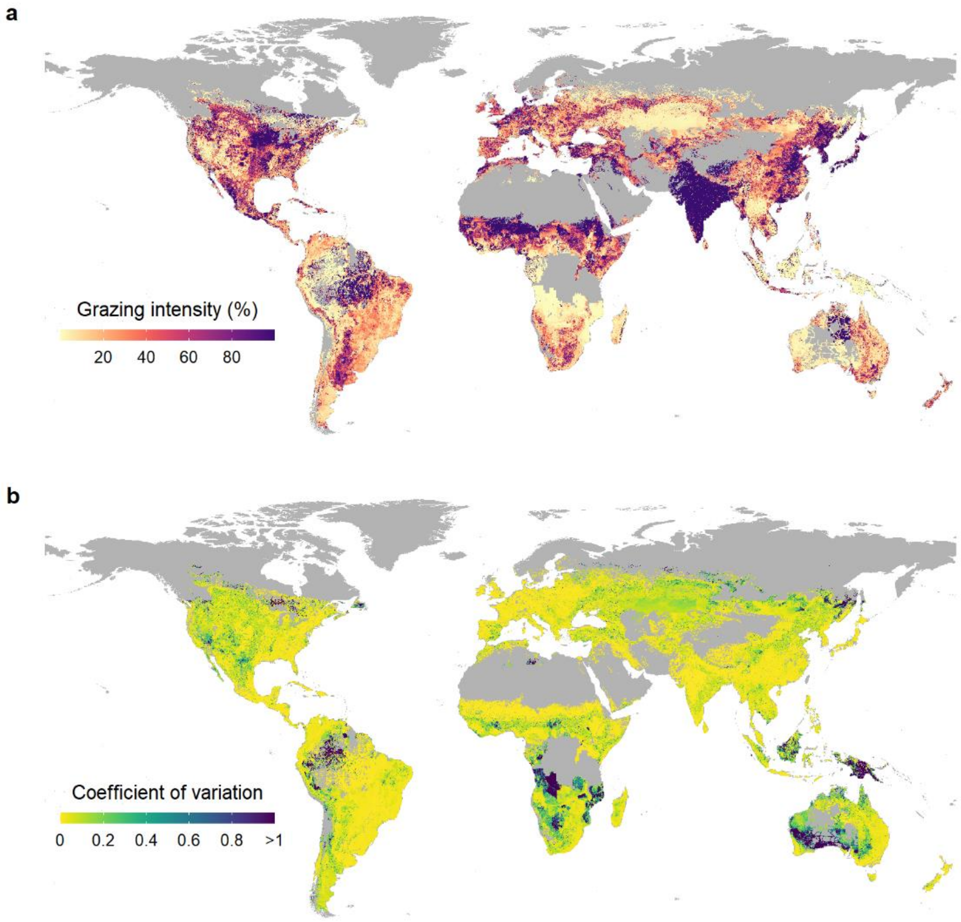

Figure S11. Global distribution of grazing intensity (a) and associated uncertainty (b). Here we used the ratio of grazed biomass to ANPP available for grazing as an indicator of grazing intensity (Methods). The coefficient of variation was calculated from the standard deviation and mean of the 400 estimates.

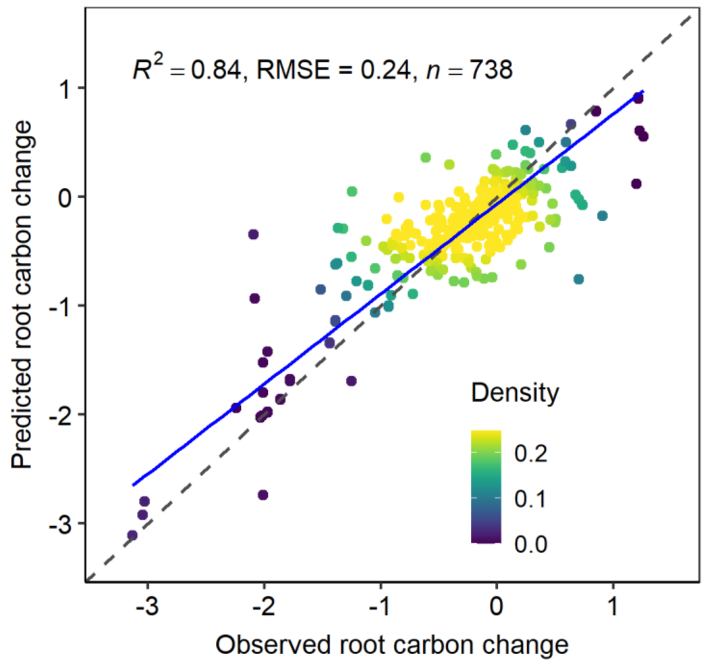

Figure S12. Heat plot showing the relationship between observed and predicted grazing-induced root carbon change (LRR). Solid line indicates fitted relationship based on ordinary least squares regression; dashed line indicates a 1:1 relationship between observed and predicted points.

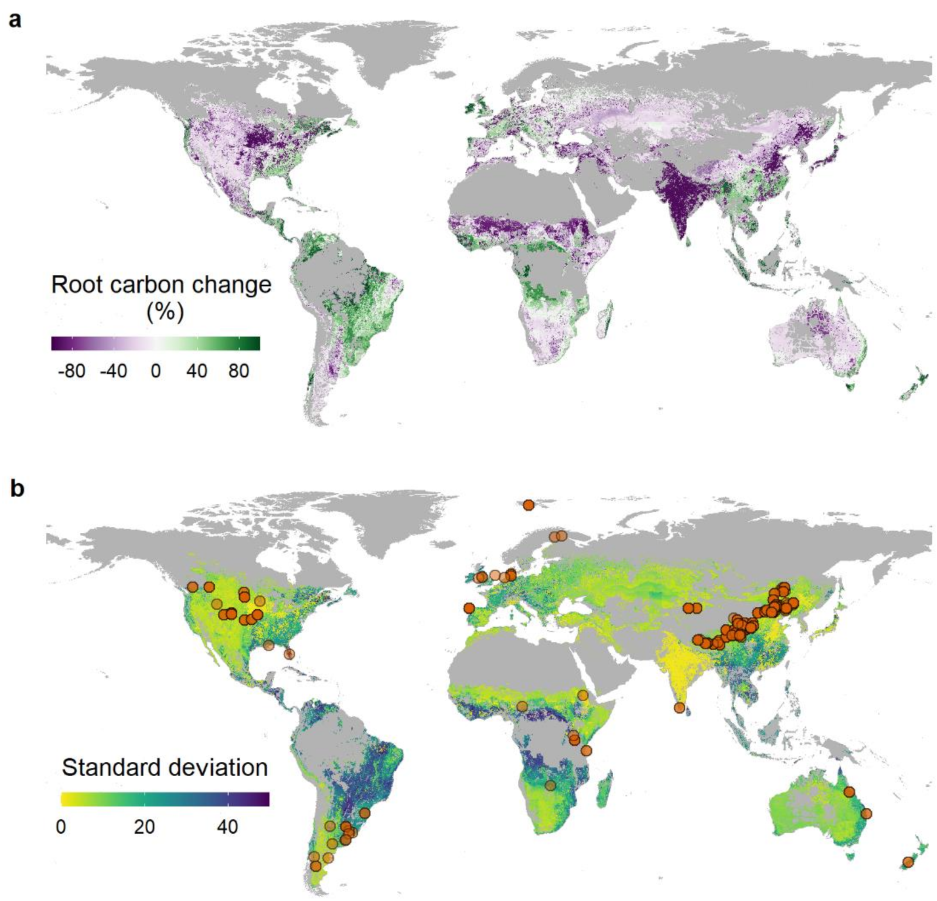

Figure S13. Global root carbon changes due to livestock grazing (a) and associated uncertainty (b). Dots in **b** represent the location of 738 paired root carbon observations from grazing studies included in the analysis.

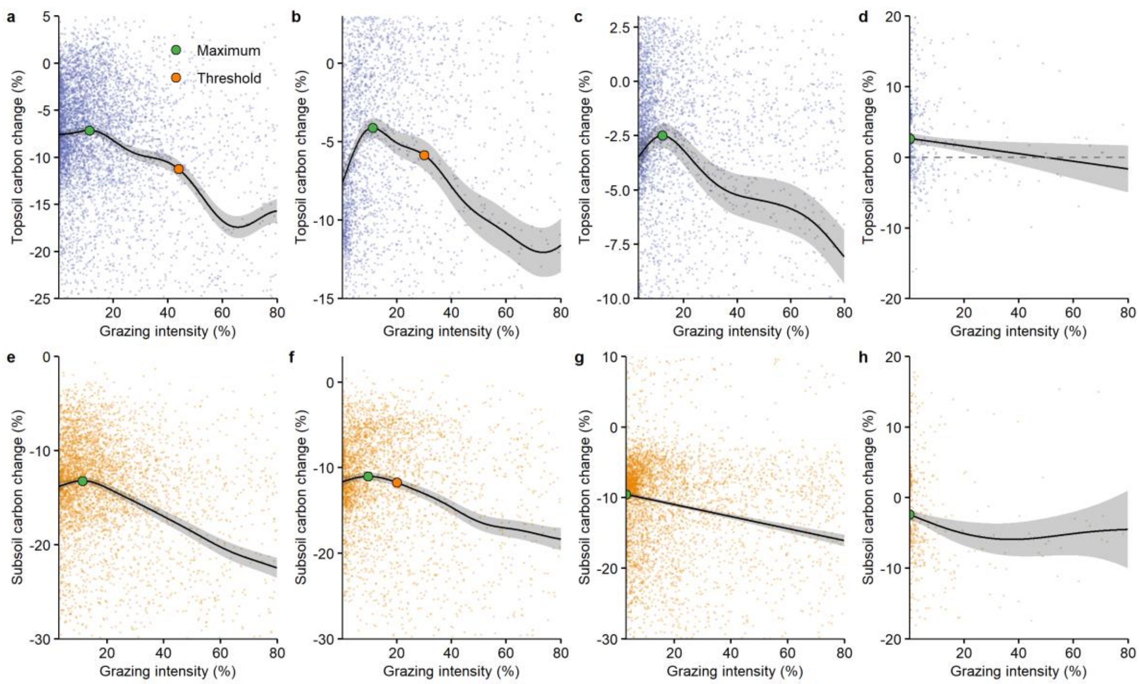

Figure S14. Nonlinear responses of soil carbon stock change to grazing intensity. a-h, The graphs show how soil carbon changes of different layers (**a-d** for topsoil, **e-h** for subsoil) respond to grazing intensity for tropical (**a, e**), subtropical (**b, f**), temperate (**c, g**), boreal (**d, h**) zones. The solid lines and shaded areas represent the smoothed trend fitted by generalized additive model and the associated 95% CI, respectively. The green points indicate the grazing intensity at which soil carbon change is predicted to be maximal, while the yellow points describe the threshold identified by the segmented regression (see Methods). Data shown here are from global estimates.

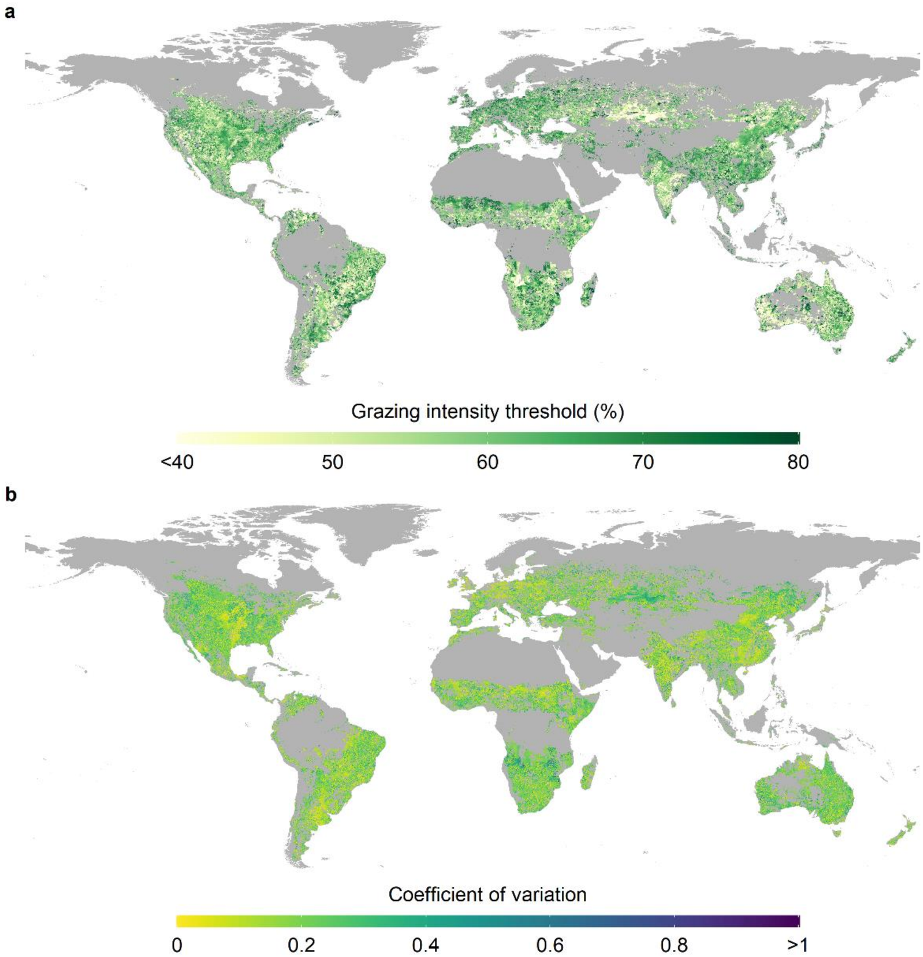

Figure S15. Global distribution of GI_{thres} (a) and associated uncertainty (b) derived from 240 estimations.

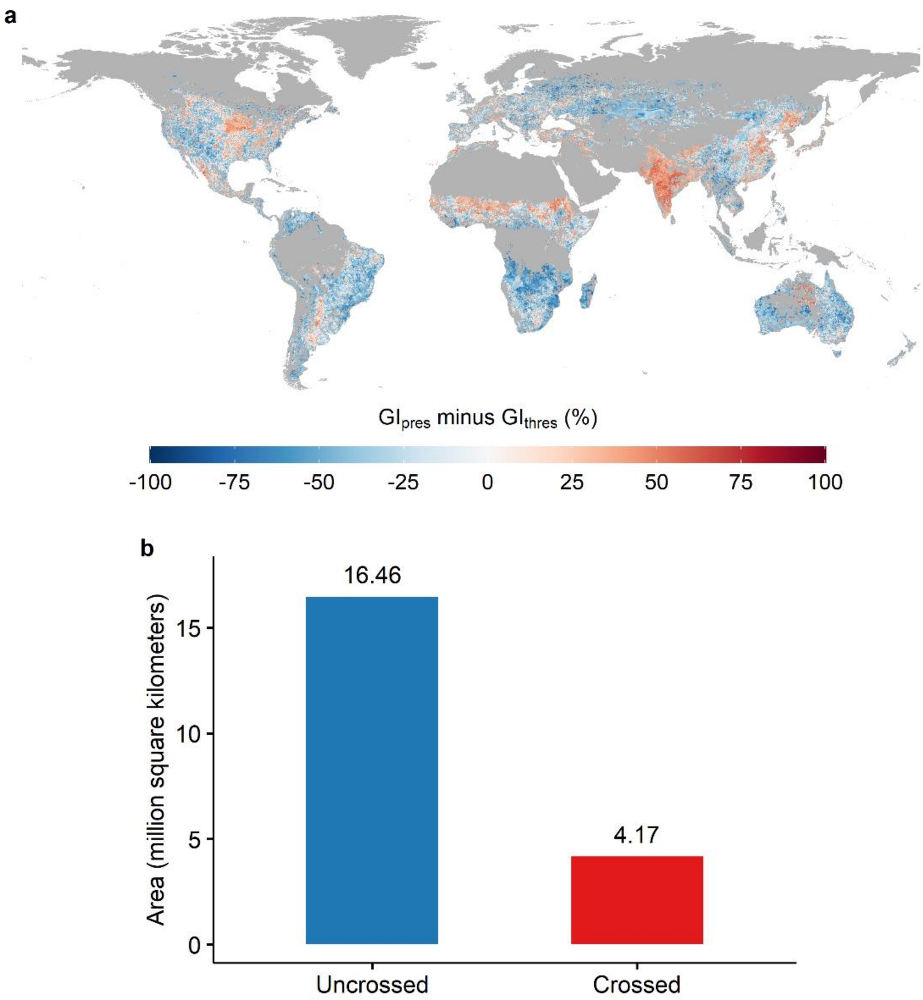

Figure S16. Comparison of current grazing intensity (GI_{pres}) with the threshold. a, Differences between GI_{pres} and GI_{thres}. **b,** Area of grazing land where GI_{pres} crossed and did not cross the threshold.

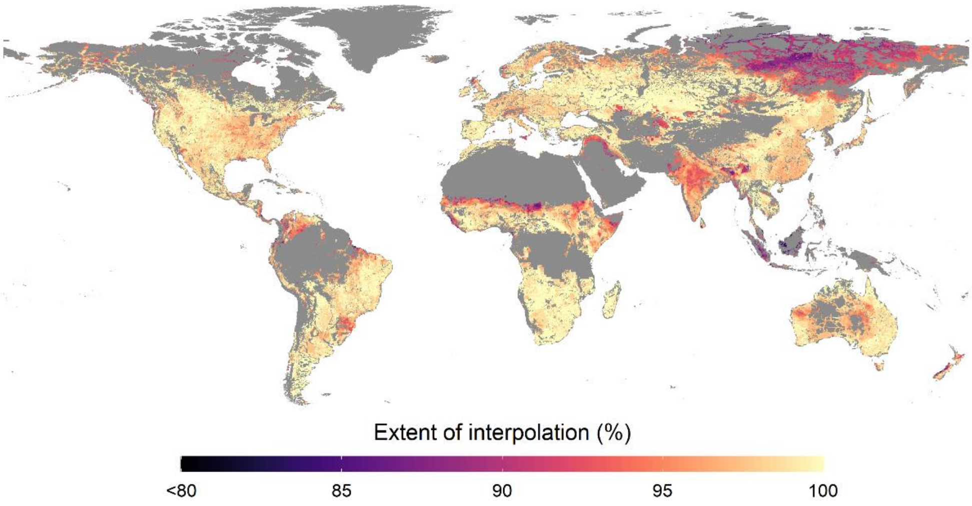

Figure S17. The extent of interpolation per pixel across all covariate layers. A value of 100 indicates that 100% of pixels fall within the sample range (see Methods).

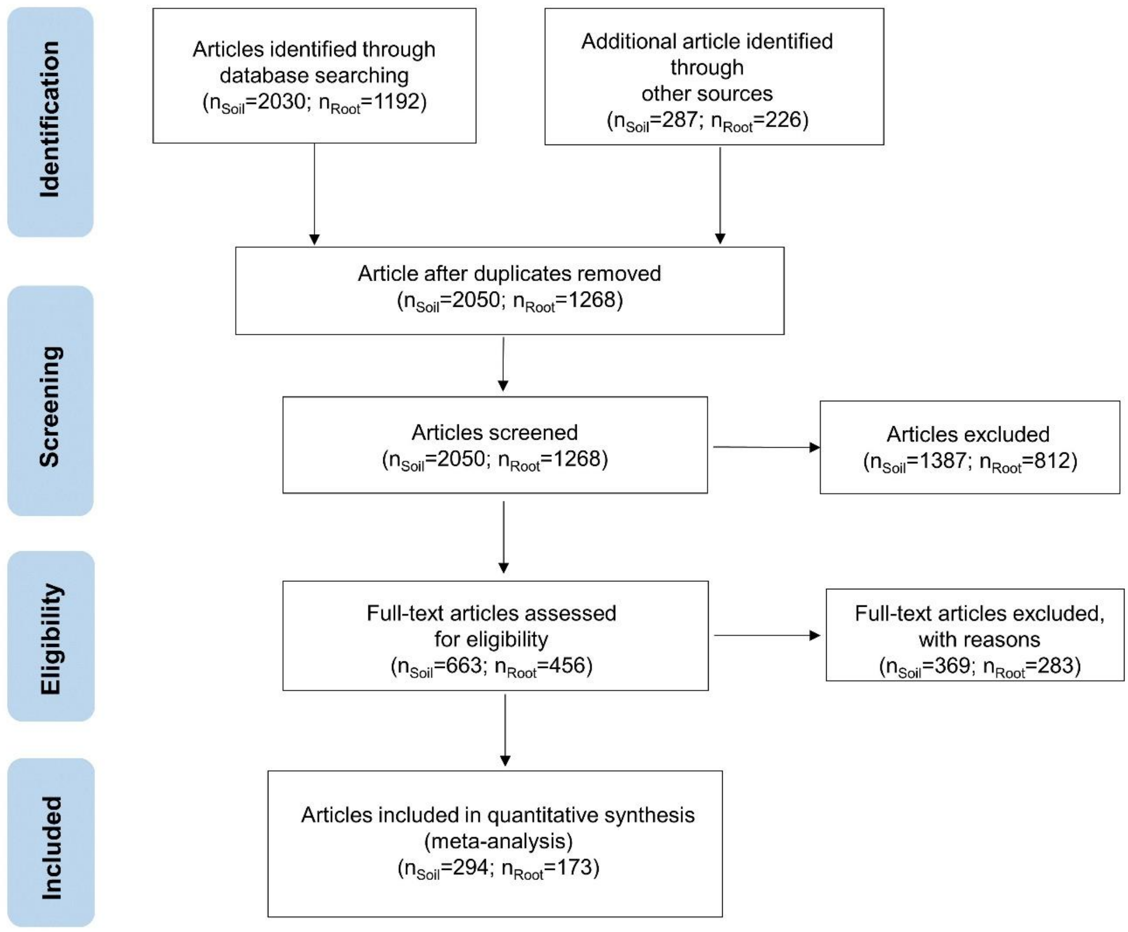

Figure S18. PRISMA flow diagram showing the procedure of selecting studies for the synthesis.

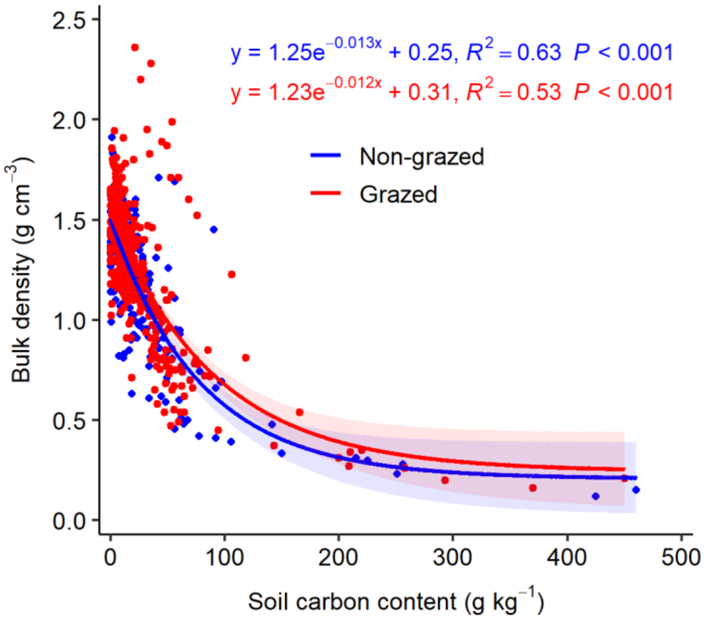

Figure S19. Relationships between soil carbon content and bulk density across grazing (n=489) and non-grazing (n=264) experiments (both *P* = 0.000). Nonlinear fits depict exponential models with shaded areas representing 95% CI. *P* values for two-tailed tests.

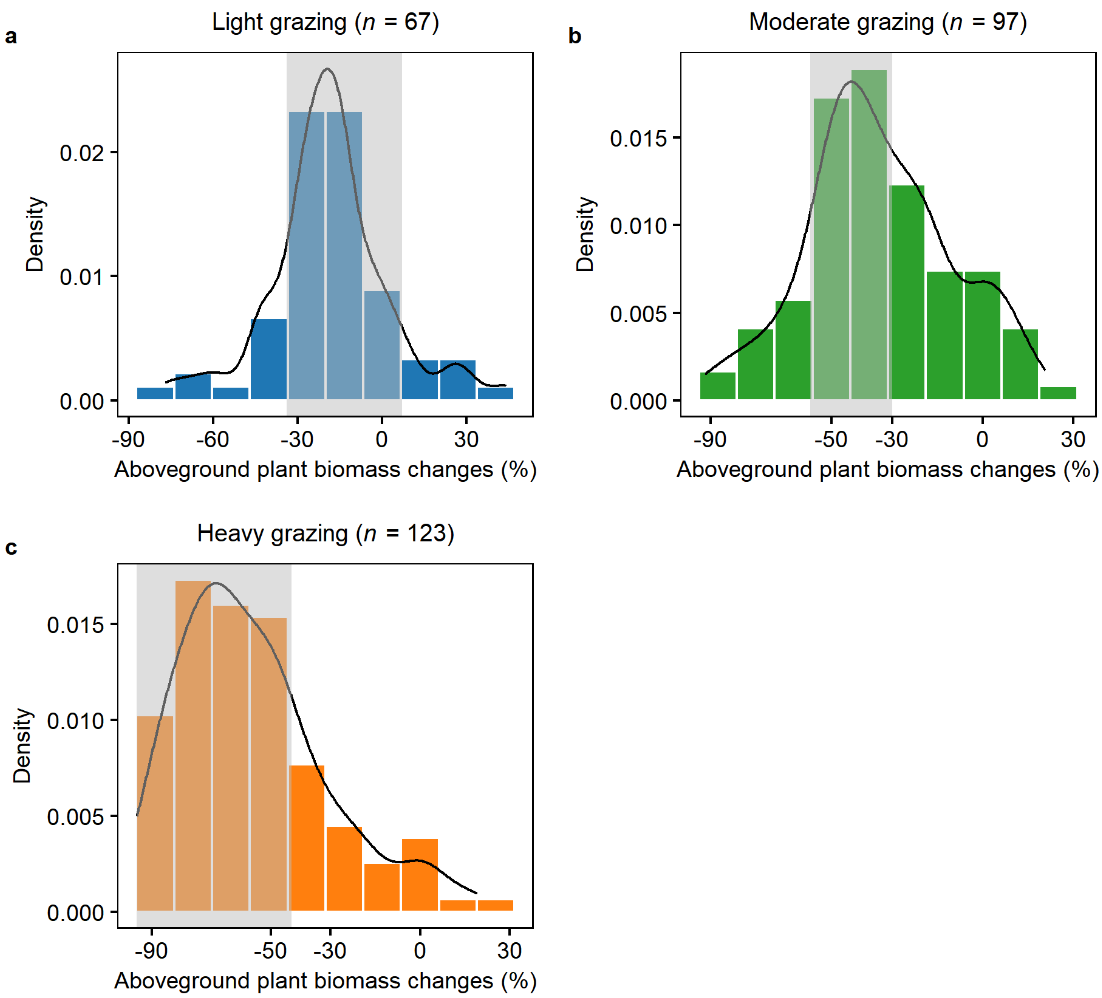

Figure S20. Histograms showing the distribution of aboveground biomass change for light (a), moderate (b) and heavy (c) grazing intensity categories. Values in parentheses are the number of experiments reporting biomass change and GI simultaneously. For each category, the shaded area indicates a higher frequency of biomass change.

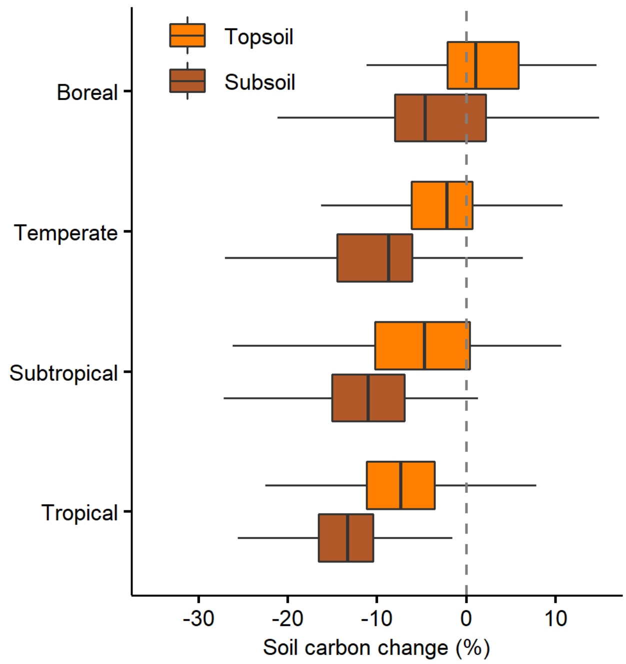

Figure S21. Boxplot of predicted relative carbon stock change (%) per soil layer and ecozone, aggregated from the spatial distributions in Figure 3 excluding grids with GI > 100%. The boxplot shows the 25th and 75th percentiles (box borders), medians (central black lines) and data ranges (whiskers).

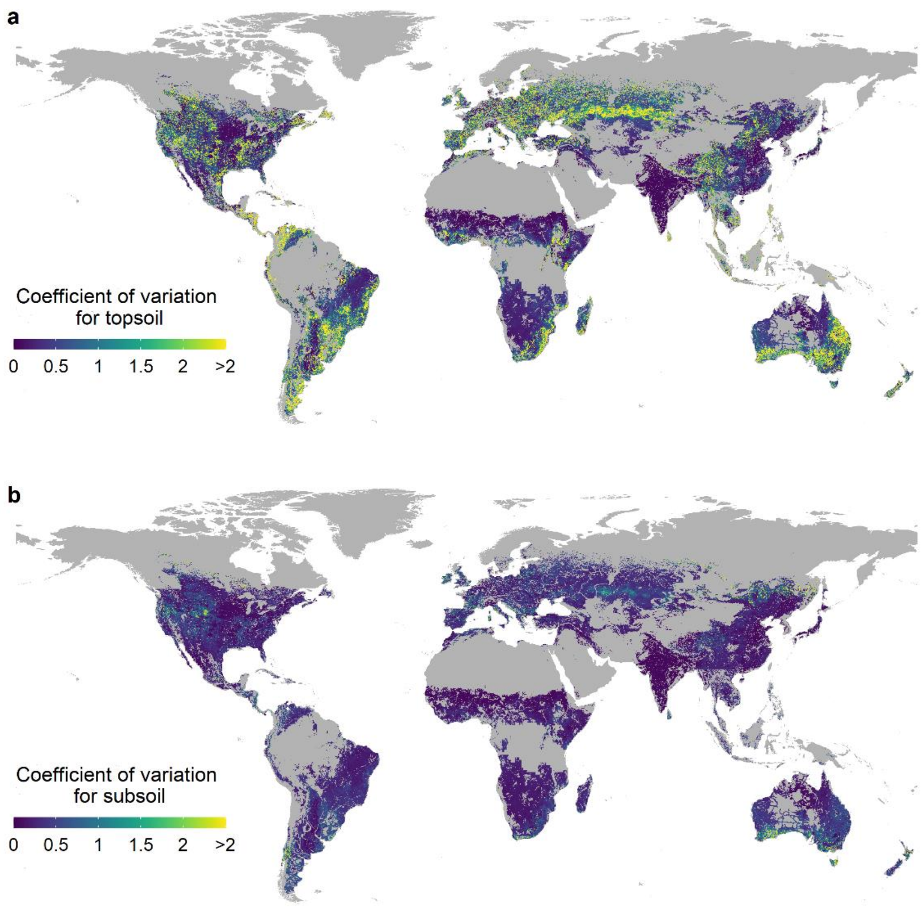

Figure S22. Uncertainties of estimated soil carbon stock changes due to grazing, derived from 100 bootstrapped predictions. The coefficient of variation was calculated as the ratio of the standard deviation to the absolute values of changes in soil carbon stocks.

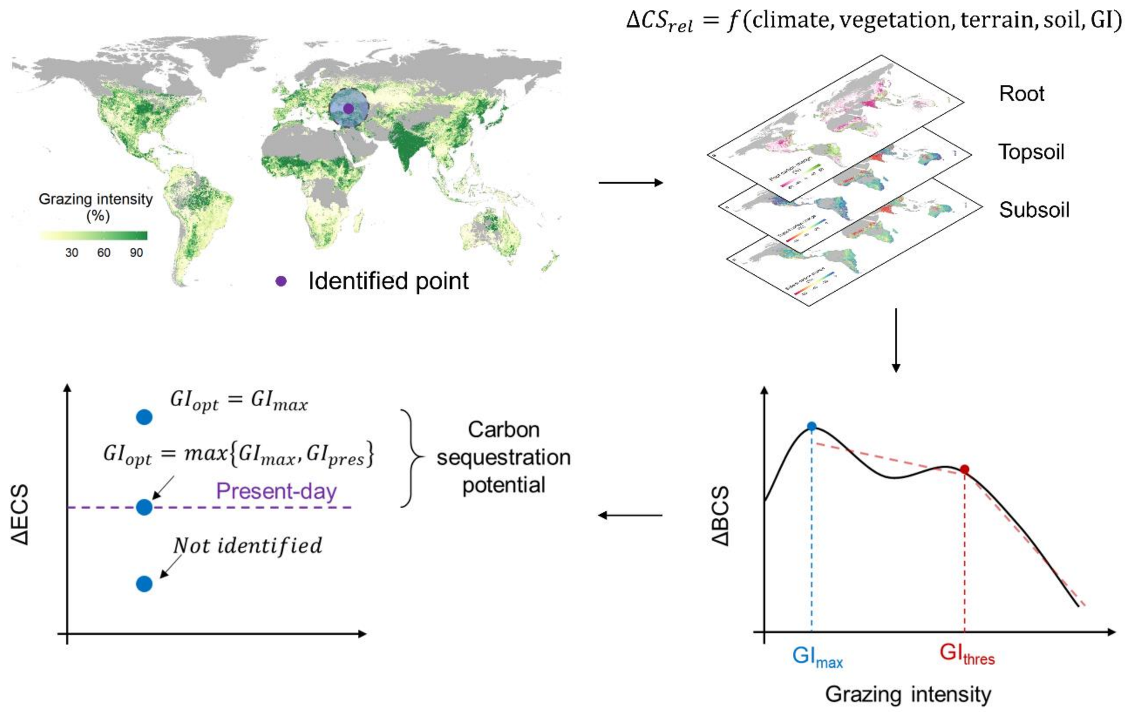

Figure S23. Illustration of the processes related to identify optimal grazing intensity (GI_{opt}) and the threshold (GI_{thres}). ΔCS_{rel} represents relative carbon stock changes. ΔBCS and ΔECD indicate changes in belowground and ecosystem carbon stocks, respectively. See Methods for more details.

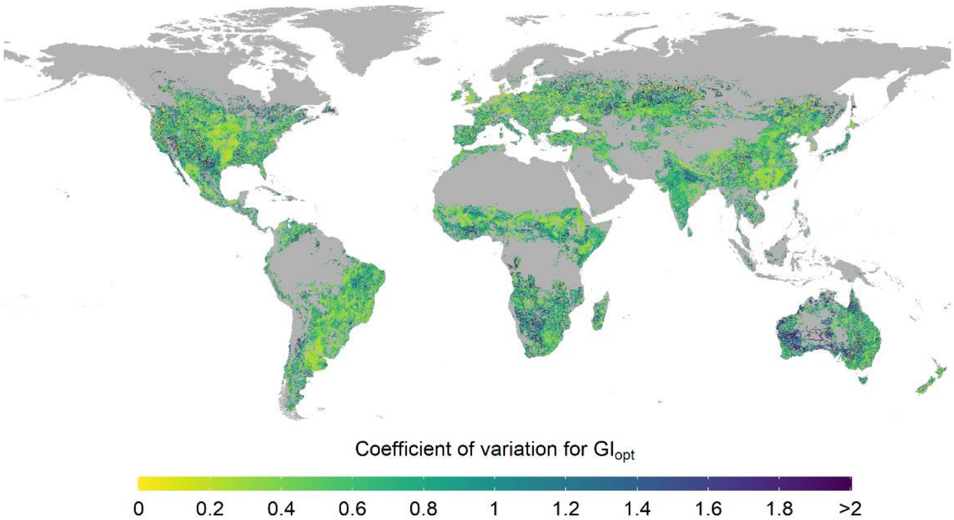

Figure S24. Uncertainty of GI_{opt} derived from 240 estimations.

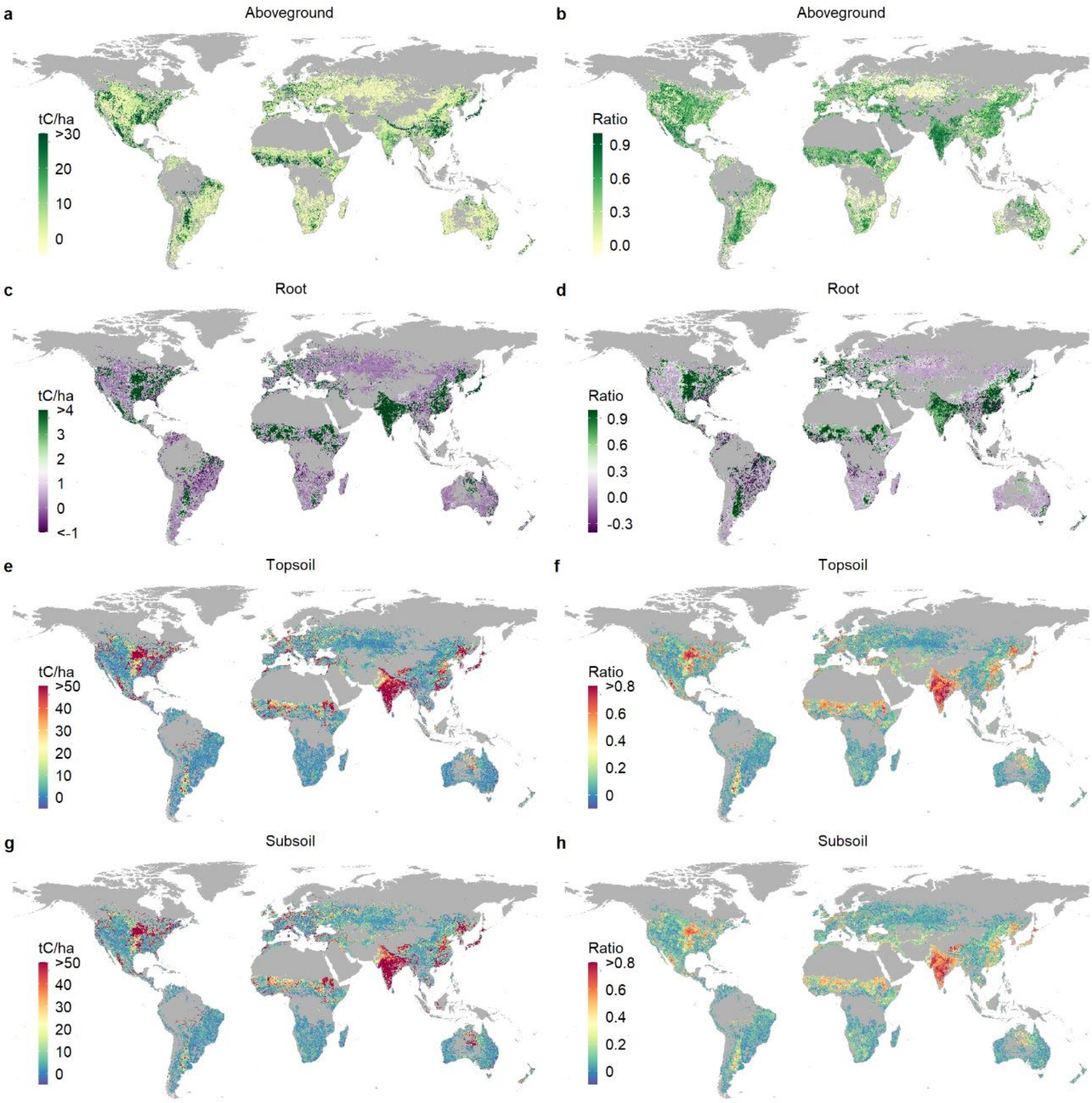

Figure S25. Global distribution of carbon sequestration potential (tC ha^{-1}) from grazing management and its contribution to current carbon stocks in aboveground biomass (a-b), root (c-d), topsoil (e-f) and subsoil (g-h). Note that due to our focus on the carbon sequestration potential of the whole ecosystem (that is, trade-offs between different carbon components) (see Methods), there are a few areas where specific carbon components would decrease under the optimal scenario.

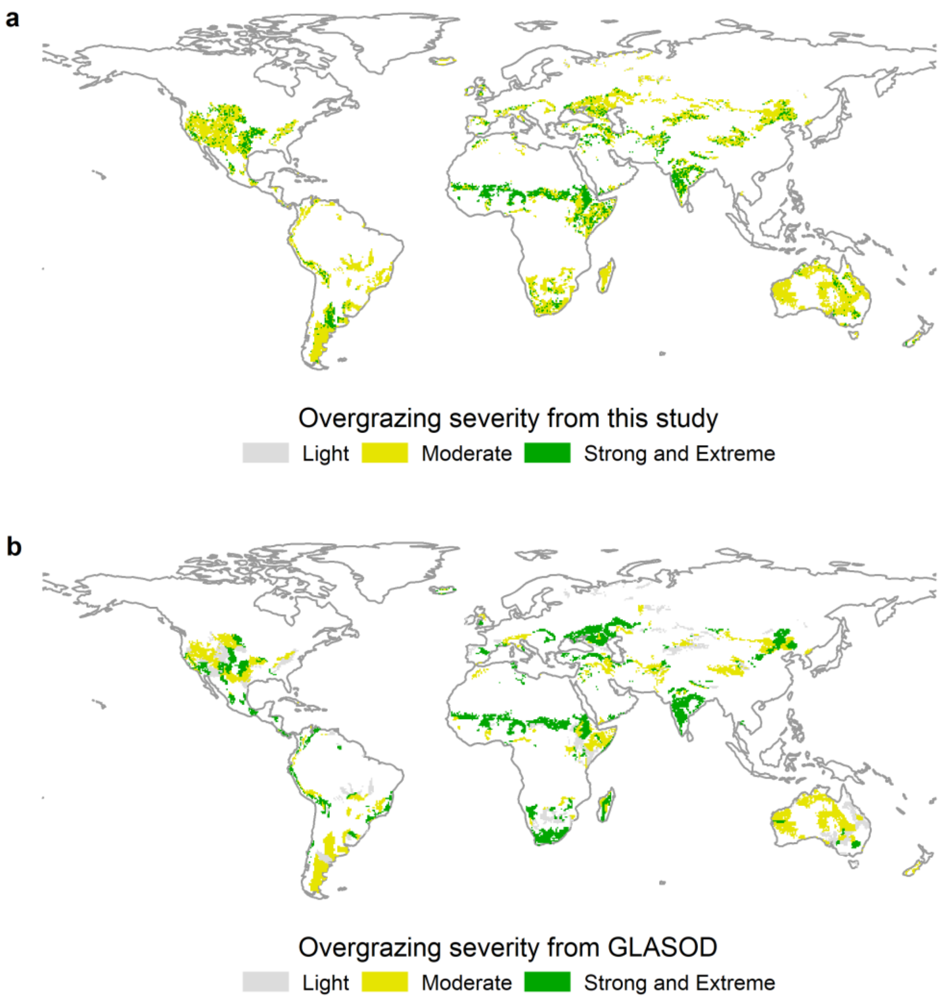

Figure S26. Overgrazing severity estimated from this study (a) and derived from the Global Assessment of Soil Degradation (GLASOD) database (b). Severity levels due to grazing are defined using a combination of the degree and the relative extent of the process.

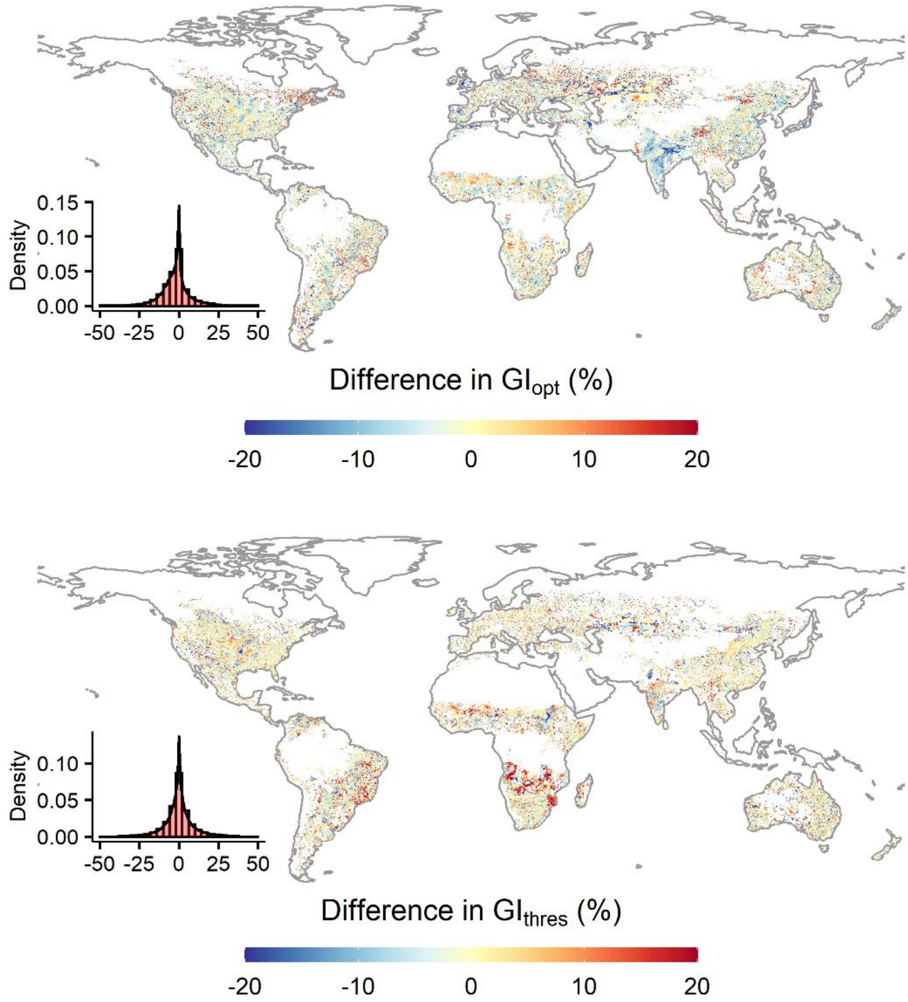

Figure S27. Differences in GI_{opt} and GI_{thres} estimates with and without consideration of local environmental conditions.

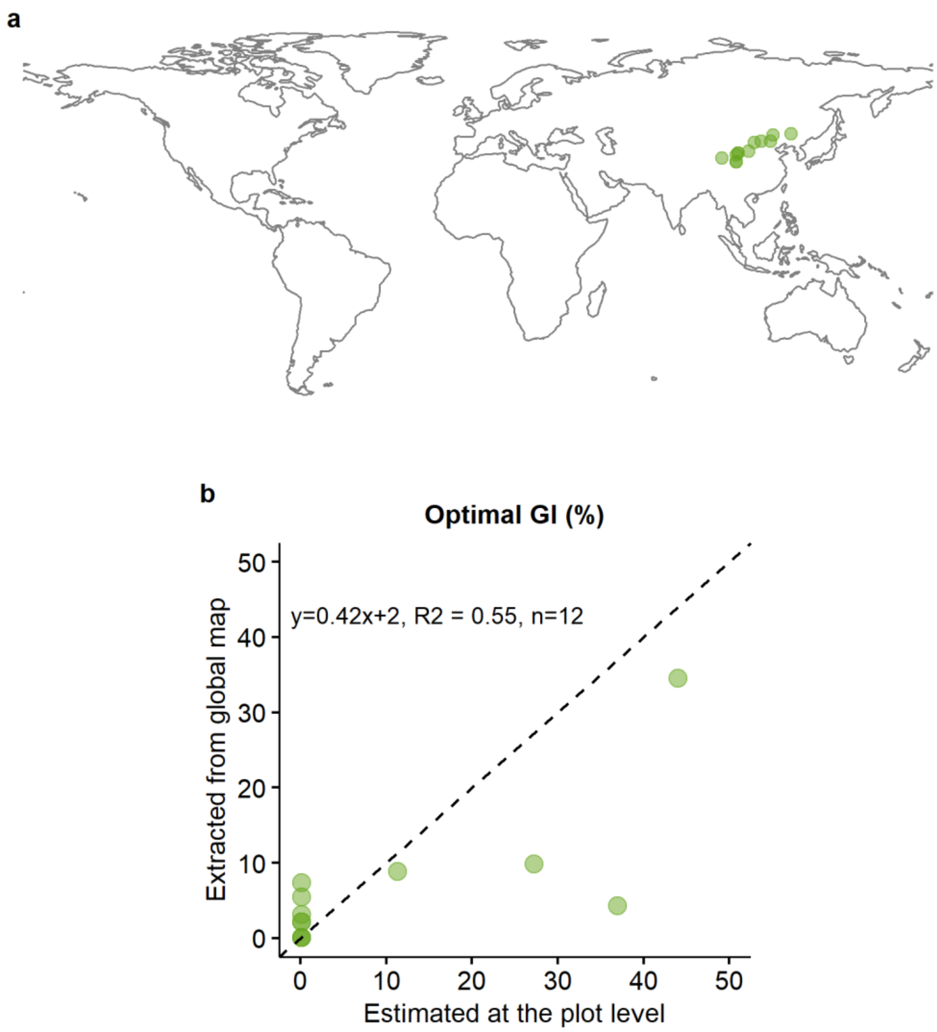

Figure S28. Comparison of plot-level GI_{opt} values with those extracted from our global optimal map.

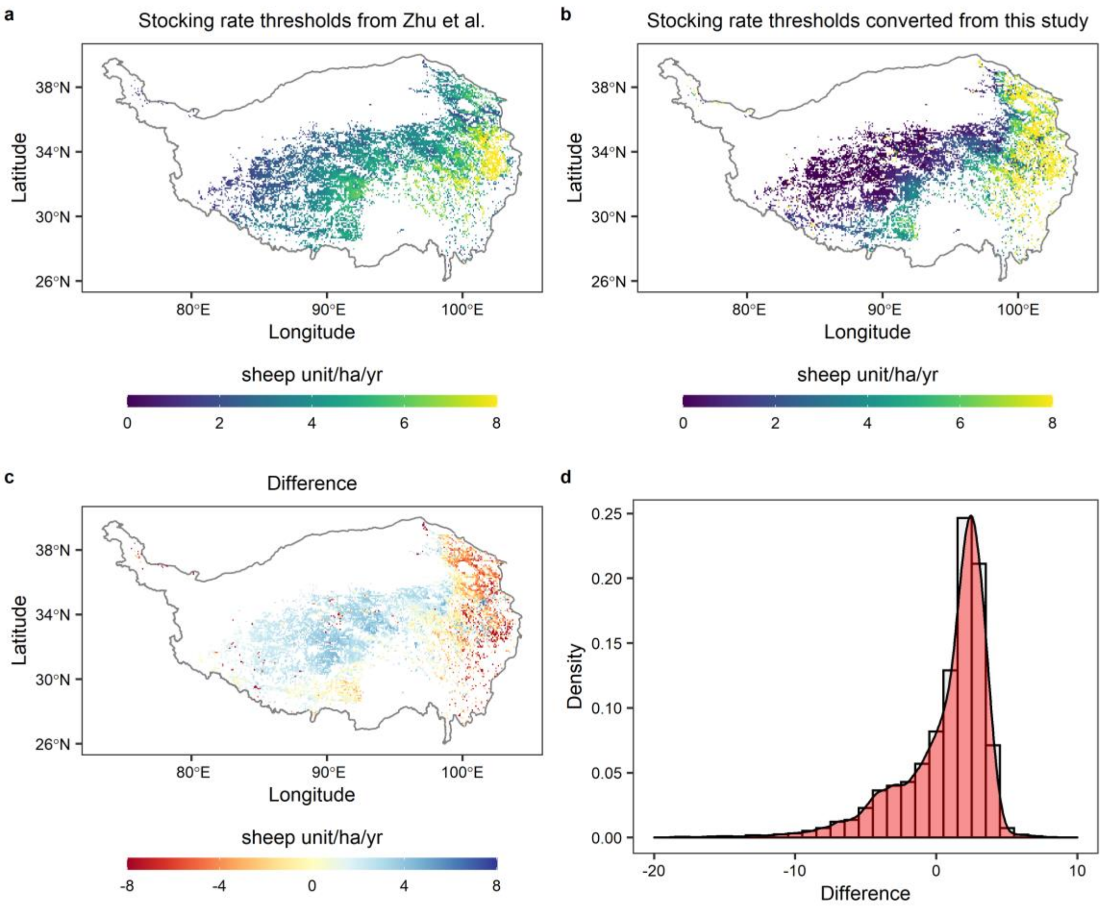

Figure S29. Comparison of stocking rate thresholds from ref.[1] with those converted from our GI_{thres} estimates over the Tibetan Plateau of China.

Table S1. The total heterogeneity (Q_T), percentage of heterogeneity due to true variation among effect sizes (I^2), between-group heterogeneity (Q_B) for soil carbon responses to grazing in the meta-analysis. k represents the number of paired observations. *P* values for two-tailed tests. Results from linear mixed-effects models

Categorical variables	k	Q_T	*P*-value for Q_T	I^2	Q_B	*P*-value for Q_B
All data	1473	39633	0.0000	0.97	-	-
MAT	1473	-	-	-	187	0.0000
MAP	1473	-	-	-	135	0.0000
Soil layer	1473	-	-	-	158	0.0000
Soil C stocks	1473	-	-	-	113	0.0000
Soil C:N	342	-	-	-	18.24	0.0004
Soil clay	119	-	-	-	23.66	0.0000
Grazing intensity category	1332	-	-	-	153	0.0000

Table S2. Grazing-driven carbon storage changes of different ecosystem components for different ecozones. Values represent means ± one standard deviation over different data sets (n = 3).

Ecozones	Predicted area (million km^2)	Carbon storage change (PgC)				
		Aboveground	Root	Topsoil	Subsoil	Total
Boreal	0.16	-0.04 ± 0.01	-0.007 ± 0.003	0.01 ± 0.006	-0.12 ± 0.05	-0.17 ± 0.05
Temperate	5.77	-2.96 ± 0.16	-1.38 ± 0.32	-4.31 ± 1.02	-8.77 ± 3.68	-17.4 ± 4.69
Subtropical	7.45	-5.05 ± 2.81	-1.42 ± 0.39	-3.45 ± 0.4	-5.82 ± 1.69	-15.7 ± 3.82
Tropical	10.2	-10.5 ± 3.41	-4.44 ± 1.86	-9.59 ± 0.96	-13.6 ± 3.04	-38.1 ± 4.27
Total	23.6	-18.5 ± 6.37	-7.26 ± 1.8	-17.3 ± 2.27	-28.4 ± 8.43	-71.5 ± 11.6

Table S3. Grazing-driven carbon sequestration potentials of different ecosystem components across different ecozones under optimal grazing scenario. Values represent means ± one standard deviation over different data sets (n = 6).

Ecozones	Opportunity area (million km^2)	Carbon sequestration potential (PgC)				
		Aboveground	Root	Topsoil	Subsoil	Total
Boreal	0.13	0.009 ± 0.014	0.008 ± 0.1	0.1 ± 0.11	0.11 ± 0.13	0.23 ± 0.25
Temperate	6.89	2.2 ± 0.27	1.74 ± 1.48	6.11 ± 2.36	6.54 ± 4.41	16.6 ± 7.42
Subtropical	5.1	3.92 ± 2.15	2.12 ± 0.33	3.41 ± 1.14	3.5 ± 2.05	12.9 ± 3.48
Tropical	8.95	8.15 ± 3.8	7.45 ± 3.13	8.2 ± 1.71	9.1 ± 5.51	32.9 ± 8.6
Total	21.1	14.3 ± 6.13	11.3 ± 5.23	17.8 ± 5.3	19.2 ± 12.4	62.6 ± 18

Table S4. Egeer's regression test and Rosenberg fail-safe numbers for publication bias. Egger's regression test was employed to detect publication bias. P-value greater than 0.05 indicates the absence of publication bias. In the presence of publication bias, the Rosenberg fail-safe numbers were utilized to further assess the potential impact of unpublished articles on the results. The results were considered susceptible to the influence of unpublished articles when the Rosenberg numbers were less than 5N+10, where N represents the number of paired observations. *P* values for two-tailed tests.

Categorical variables	N	Z value for Egger's test	P value for Egger's test	Rosenberg fail-safe number	5N+10
All data	1473	-4.1	0.00	1262001	7375
MAT	1473	-3.25	0.00	1262001	7375
MAP	1473	-3.95	0.00	1262001	7375
Soil layer	1473	-3.27	0.001	1262001	7375
Soil C stocks	1473	-4.17	0.00	1262001	7375
Soil C:N	342	-2.24	0.02	40956	1720
Soil clay	119	-1.59	0.11	12402	605
Grazing intensity category	1332	-2.27	0.02	826422	6670

Table S5. Information on the 84 selected covariate layers.

ID	Group	Variable	Unit	Resolution	ref
1	Atmosphere	Annual mean radiation	W m^{-2}	≈18.5km	2
2	Atmosphere	Highest weekly radiation	W m^{-2}	≈18.5km	
3	Atmosphere	Lowest weekly radiation	W m^{-2}	≈18.5km	
4	Atmosphere	Radiation seasonality (C of V)	W m^{-2}	≈18.5km	
5	Atmosphere	Radiation of wettest quarter	W m^{-2}	≈18.5km	
6	Atmosphere	Radiation of driest quarter	W m^{-2}	≈18.5km	
7	Atmosphere	Radiation of warmest quarter	W m^{-2}	≈18.5km	
8	Atmosphere	Radiation of coldest quarter	W m^{-2}	≈18.5km	
9	Atmosphere	Annual mean moisture index	-	≈18.5km	
10	Atmosphere	Highest weekly moisture index	-	≈18.5km	
11	Atmosphere	Lowest weekly moisture index	-	≈18.5km	
12	Atmosphere	Moisture index seasonality (C of V)	-	≈18.5km	
13	Atmosphere	Mean moisture index of wettest quarter	-	≈18.5km	
14	Atmosphere	Mean moisture index of driest quarter	-	≈18.5km	
15	Atmosphere	Mean moisture index of warmest quarter	-	≈18.5km	
16	Atmosphere	Mean moisture index of coldest quarter	-	≈18.5km	
17	Atmosphere	Nitrogen deposition	$mgN/m^2/yr$	3.75°	3
18	Climate	Annual Mean Temperature	°C	≈1km	4
19	Climate	Mean Diurnal Range	°C	≈1km	
20	Climate	Isothermality	%	≈1km	
21	Climate	Temperature Seasonality (C of V)	°C	≈1km	
22	Climate	Max Temperature of Warmest Month	°C	≈1km	
23	Climate	Min Temperature of Coldest Month	°C	≈1km	
24	Climate	Temperature Annual Range	°C	≈1km	
25	Climate	Mean Temperature of Wettest Quarter	°C	≈1km	
26	Climate	Mean Temperature of Driest Quarter	°C	≈1km	
27	Climate	Mean Temperature of Warmest Quarter	°C	≈1km	
28	Climate	Mean Temperature of Coldest Quarter	°C	≈1km	
29	Climate	Annual Precipitation	mm	≈1km	
30	Climate	Precipitation of Wettest Month	mm	≈1km	
31	Climate	Precipitation of Driest Month	mm	≈1km	
32	Climate	Precipitation Seasonality (C of V)	mm	≈1km	
33	Climate	Precipitation of Wettest Quarter	mm	≈1km	
34	Climate	Precipitation of Driest Quarter	mm	≈1km	
35	Climate	Precipitation of Warmest Quarter	mm	≈1km	
36	Climate	Precipitation of Coldest Quarter	mm	≈1km	
37	Climate	Arid index	-	≈1km	5
38	Climate	Evapotranspiration	mm/yr	≈1km	
39	Soil	Permaforst attribute	-	0.1°	6

40	Soil	Bulk density	cg/cm^3	≈1km	7
41	Soil	Cation exchange capacity	mmol(c)/kg	≈1km	
42	Soil	Coarse fragments	cm^3/dm^3	≈1km	
43	Soil	Nitrogen	mg/kg	≈1km	
44	Soil	Clay content	g/kg	≈1km	
45	Soil	Sand content	g/kg	≈1km	
46	Soil	Silt content	g/kg	≈1km	
47	Soil	pH	-	≈1km	
48	Soil	Organic carbon	dg/kg	≈1km	
49	Soil	C:N	-	≈1km	
50	Soil	Soil order (USDA)	-	≈1km	
51	Soil	Total S	%	≈1km	8
52	Soil	CaCO3	%	≈1km	
53	Soil	Gypsum	%	≈1km	
54	Soil	Electrical conductivity	ds/m	≈1km	
55	Soil	Exchangeable calcium	cmol/kg	≈1km	
56	Soil	Exchangeable magnesium	cmol/kg	≈1km	
57	Soil	Exchangeable sodium	cmol/kg	≈1km	
58	Soil	Exchangeable potassium	cmol/kg	≈1km	
59	Soil	Exchangeable aluminum	cmol/kg	≈1km	
60	Soil	Base saturation	%	≈1km	
61	Soil	Gravel content	%	≈1km	
62	Soil	Total phosphorus	%	≈1km	
63	Soil	Total potassium	%	≈1km	
64	Soil	Microbial biomass carbon (MBC)	gC/m^2	0.5°	9
65	Soil	Microbial biomass nitrogen (MBN)	gN/m^2	0.5°	
66	Soil	MBC:MBN	-	0.5°	
67	Soil	Bacterial biomass carbon	gC/m^2	0.5°	10
68	Soil	Fungal biomass carbon	gC/m^2	0.5°	
69	Soil	F/B ratio	-	0.5°	
70	Soil	Nematode abundance	number/100g	≈1km	11
71	Soil	Soil depth	cm	-	-
72	Vegetation	Land cover	-	≈500m	12
73	Vegetation	Normalized Difference Vegetation Index	-	≈250m	13
74	Vegetation	Arbuscular mycorrhizal	%	≈18.5km	14
75	Vegetation	Ectomycorrhizal	%	≈18.5km	
76	Vegetation	Ericoid mycorrhizal	%	≈18.5km	
77	Vegetation	Non-mycorrhizal	%	≈18.5km	
78	Topography	Northess	-	≈30m	15
79	Topography	Eastness	-	≈30m	
80	Topography	Hill	-	≈30m	
81	Topography	Slope	degree	≈30m	
82	Topography	Elevation	m	≈30m	

83	Anthropogenic	Grazing intensity category	-	≈1km	This study
84	Anthropogenic	Grazing intensity	%	≈1km	

References

1 Zhu Q, Chen H, Peng C, et al. An early warning signal for grassland degradation on the Qinghai-Tibetan Plateau. Nature Communications, 14(1), 6406 (2023).

2 Kriticos, D. J. et al. CliMond: global high-resolution historical and future scenario climate surfaces for bioclimatic modelling. Methods in Ecology and Evolution 3, 53-64 (2012).

3 Galloway, J. N. et al. Nitrogen cycles: past, present, and future. Biogeochemistry 70, 153-226 (2004).

4 Fick, S. E. & Hijmans, R. J. WorldClim 2: new 1-km spatial resolution climate surfaces for global land areas. International journal of climatology 37, 4302-4315 (2017).

5 Zomer, R. J., Xu, J. & Trabucco, A. Version 3 of the global aridity index and potential evapotranspiration database. Scientific Data 9, 1-15 (2022).

6 Brown, J., Ferrians Jr, O., Heginbottom, J. A. & Melnikov, E. Circum-arctic map of permafrost and ground ice conditions. (1997).

7 Hengl, T. et al. SoilGrids250m: Global gridded soil information based on machine learning. PLoS one 12, e0169748 (2017).

8 Shangguan, W., Dai, Y., Duan, Q., Liu, B. & Yuan, H. A global soil data set for earth system modeling. Journal of Advances in Modeling Earth Systems 6, 249-263 (2014).

9 Xu, X., Thornton, P. E. & Post, W. M. A global analysis of soil microbial biomass carbon, nitrogen and phosphorus in terrestrial ecosystems. Global Ecology and Biogeography 22, 737-749 (2013).

10 He, L. et al. Global biogeography of fungal and bacterial biomass carbon in topsoil. Soil Biology and Biochemistry 151, 108024 (2020).

11 Van Den Hoogen, J. et al. Soil nematode abundance and functional group composition at a global scale. Nature 572, 194-198 (2019).

12 Friedl, M. et al. ISLSCP II MODIS (Collection 4) IGBP Land Cover, 2000-2001. ORNL DAAC (2010).

13 Didan, K., Munoz, A. B., Solano, R. & Huete, A. MODIS vegetation index user's guide (MOD13 series). University of Arizona: Vegetation Index and Phenology Lab (2015).

14 Soudzilovskaia, N. A. et al. Global mycorrhizal plant distribution linked to terrestrial carbon stocks. Nature communications 10, 1-10 (2019).

15 Rabus, B., Eineder, M., Roth, A. & Bamler, R. The shuttle radar topography mission—a new class of digital elevation models acquired by spaceborne radar. ISPRS journal of photogrammetry and remote sensing 57, 241-262 (2003).